

Answer to editor

We thank the editor for her careful reading of the manuscript and constructive remarks. In the manuscript we identified all changes in response to the editor suggestions in **red bold**.

General comments

We tried to improve the discussion of our results and the summary and conclusion section and incorporated all suggestions to streamline the text.

LN: 223

The RASM ensemble forecast simulations were carried out from 1st November 2019 through 30th April 2020. Each ensemble member was initialized with the same sea ice and ocean conditions and on the same date, but then it was forced by a different, 24-hr apart, NCEP forecast data set which was initialized at 00.00 between 1st and 31st October 2019. The 30-member RASM ensemble was forced with different lateral boundary conditions from 9-months forecast of the NCEP climate forecast system, applying a linear nudging of temperature, zonal- and meridional wind above 500 hPa.

LN: 624

The internally generated sea ice volume differences among the 30 ensemble members for the Arctic domain are in the range of 1000 km³ and indicate strong internally generated variability due to Arctic feedbacks and remote impacts from the mid-latitudes. Some ensemble members develop positive ice volume differences and others negative differences relative to the ensemble mean. The great positive sea ice thickness anomaly in the Barents Sea during winter 2020 was connected to an enhanced ice growth following the colder temperature anomalies in this area, and a result of greater sea ice convergence and ice shears.

Minor:

We accepted all suggestions and corrected all sentences.

The SIMS measurements were independent of the ASSIST protocol, but in general agreement with the visual observations. However, the ASSIST observations are prone to large errors because visual ice thickness observations were near to impossible due to the darkness of the polar night and due to the 100% ice coverage which prevented broken floes from tipping over.

We would like to keep the preview of upcoming chapters.

December 2019 was not shown simply to save space.

The underestimation of the ship based EM measurements and the correction of biases due to extensive ramming is under way and subject of another study by Haas et al. (in prep.) about the midwinter voyages of “RV Kapitan Dranitzyn” which we hope to submit by the end of the year.

We replotted Fig. 10 and show convergence, divergence and shear anomaly plots.

We replotted Fig. 11 with the same isoline intervals.

We introduced the requested citations.

We removed the redundant subcaptions in Fig. 5, 10, 11, 15 and 16.

We would like to keep the subcaptions in Fig. 7.

We would like to keep also Fig. 12 in accordance with one reviewer.

Leads have been visually identified in the VIIRS.

Fig. 9b shows the RASM daily mean sea ice divergence simulated on 3/5/2020, No data manipulation was done except the daily averaging, which is performed within the CICE code for specified temporal output.

The three panels of Fig. 10 show sea ice anomalies calculated from the RASM hindcast simulation for January-March (JFM) 2020 compared to the RASM climate mean JFM 2010-2019 for negative divergence (top; blue shading represents less divergence) and positive divergence (middle; red shading represents more divergence). The bottom graph displays ice shear anomalies (%/day). The mean velocity vectors for the same period of JFM 2020 are overlaid in each plot.

Answers to reviewer 1

We thank the reviewer for his/her constructive remarks. In the manuscript we identified all changes in response to the reviewer in **black bold**.

General comments

Figures 4, 7, and 16 were replotted and enlarged as suggested.

Figures 2, 3, and 5 were replotted to be similar to Fig. 12 as suggested.

Figs. 10 and 11 are vector plots and a polar-stereographic projection doesn't work well due to the convergence of meridians toward the pole. Fig. 10 was replotted.

We explained all abbreviations about the Target and Taylor diagrams in Fig. 6 by improved figure caption: **Figure 6. Target diagram (a) of normalised bias and normalized unbiased root-mean-square difference (uRMSD) and Taylor diagram (b) of normalised standard deviation and correlation between the RASM sea ice thickness simulations and CryoSat2/SMOS data from November 2019 to March 2020. The square marker indicates the reference (REF) value, i.e., perfect model.**

We introduced the following sentences for description of the Target and Taylor diagrams: **RASM skill is assessed using the Target diagram (Jolliff et al., 2009) to visualise root-mean-square difference (RMSD; distance from a center), unbiased RMSD (uRMSD; x-axis), and bias (y-axis) for monthly SIT on a single plot. They are normalised by the standard deviation of CryoSat2/SMOS SIT. The Taylor diagram (Taylor, 2001) provides an additional set of statistics in uRMSD by displaying the correlation and the ratio of the standard deviation between RASM and CryoSat2 SIT**

We added the following citations:

Jolliff, J. K., et al. ,2009, Summary diagrams for coupled hydrodynamic ecosystem model skill assessment, J. Mar. Syst., 76, 64–82.

Taylor, K. E., 2001, Summarizing multiple aspects of model performance in a single diagram, J. Geophys. Res., 106, 7183–7192.

Summary and conclusion sections were partly revised.

Specific comments:

LN 165-167: We described the concept in the text. **The concept is described by Ricker (2020) in the CryoSat2-SMOS merged product description document. An optimal interpolation scheme (OI) has been used, that allows the merging of datasets from diverse sources on a predefined analysis grid. The data are weighted differently based on known uncertainties of the individual products and an estimated correlation length scale. OI minimizes the total error of observations with respect to a background field and provides ideal weighting for the observations at each grid cell. The background field consists of a weighted average of CryoSat-2 and SMOS data two weeks before and after the rolling observation period with a length of 7 days. The CryoSat2-SMOS product is then defined as the sea-ice thickness analysis fields of the 7 day observation period with the center date as the reference time of each file. Melting does not allow to**

retrieve sea-ice thickness estimates from CryoSat-2 and SMOS during summer between May and September. Therefore, the merged product is limited to the period from mid-October to mid-April only due to the background field requirement.

LN 208: Title of section 3.1 was changed to: **3.1 Analysis of atmospheric and sea ice conditions in ERA5 and satellite data**

LN 216: In Fig. 1a we explain the AO time series and in Fig. 1b the spatial AO pattern. We explain with the following text why Fig. 1b is based on ERA-5 1979-2000.

Figure 1a presents daily values of the AO index in mean sea level pressure (SLP) based on ERA-5 from October 2019 until May 2020 with 7-day running mean (red line) and Fig. 1b the spatial AO pattern north of 20 °N. The AO pattern was defined as the leading mode of Empirical Orthogonal Function analysis of monthly mean SLP during the 1979-2000 period over the domain 20°-90°N. This domain and reference period was used for the calculation of the spatial AO patterns to ensure a comparability with the widely used AO index provided by the NOAA Climate Prediction center (CPC, https://www.cpc.ncep.noaa.gov/products/precip/CWlink/daily_ao_index/ao.shtml), which is based on the AO pattern calculated for the mentioned reference period and NCEP/NCAR reanalysis data set. The daily AO indices (Fig. 1a) have been obtained by projecting ERA5 daily SLP data from 1979 to May 2020 onto the AO pattern shown in Fig. 1b. For comparison the loading pattern of the AO for the different ERA-5 reference period 2010-2019 was computed (not shown), and the corresponding AO index for the MOSAiC period, obtained by projecting the daily SLP anomalies onto this loading pattern. The time series of daily values of the AO index from October 2019 to April 2020 obtained by projecting the daily SLP anomalies onto the loading pattern from 2010-2019 agree entirely with Fig 1a.

For the information of the reviewer (not presented in the manuscript), we display in Fig. R1a the AO pattern for the period 2010-2019 and in Fig. R1b the AO time series of by projecting onto the loading pattern shown in Fig. R1a.

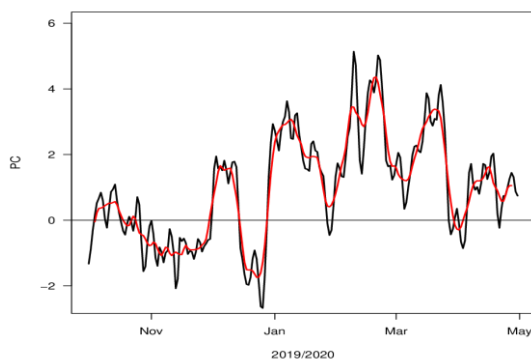


Fig. R1a. Time series of daily values of the AO index from October 2019 to April 2020 (black line) with 7-day running mean (red line), obtained by projecting the daily SLP anomalies onto the loading pattern shown in Fig. R1b.

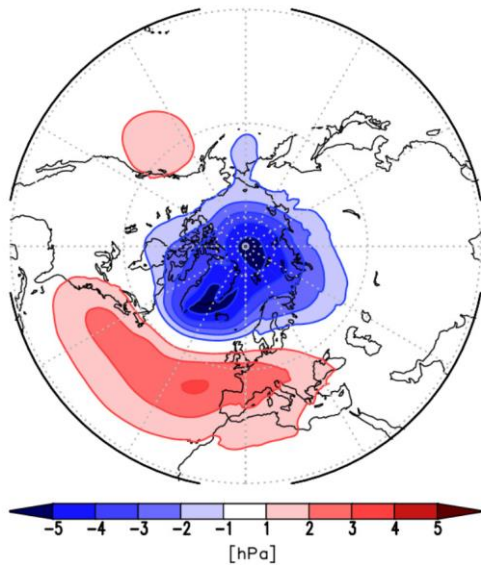


Figure R1b. Loading pattern of AO based on monthly mean SLP for the period 2010-2019 (ER5 data).

LN 219: Fig. 2 was revised

LN 255-257: Figs. 3 and 4 have been replotted using the same color bars. The mentioned sentence was changed to: **The largest positive thickness anomalies between 1.0 and 1.5 m occur in the BS, along the north-eastern Canadian coast and in the central Arctic Ocean.**

LN 265-267: The sentence was changed to:

The differences in SIT (Fig. 5) may be partly connected to the impact of surface roughness on the radar freeboards and the retrieval algorithms as discussed by Landy et al. (2020). Specifically, the merged CryoSat-2/SMOS SIT data is dominated by the CryoSat-2 radar altimeter contribution in areas with multi-year sea ice. Radar freeboard is the term in sea ice radar altimetry that describes the height of the ice surface above local sea level perceived by a radar altimeter. It differs from sea ice freeboard, the actual height of the ice surface, by a correction that requires prior knowledge of snow depth and density. The purpose of this correction is to remove the impact of the slower wave propagation speed of the radar pulse within the snow layer on the radar range and thus ice surface elevation. The corrected radar freeboard is then converted to sea ice thickness using information of the densities of sea ice, ocean water, and snow, and estimating the depth of snow accumulated on the ice surface based on climatological values (Hendricks et al. 2020). In Landy et al. (2020) it is demonstrated that sea ice surface roughness may cause a systemic radar freeboard uncertainty which represents one of the principal sources of pan-Arctic SIT uncertainty. In the CryoSat-2 retrieval algorithm of the CryoSat-2/SMOS SIT data set this systemic bias might contribute to the higher CryoSat-2/SMOS thicknesses in the central Arctic and specifically north of the Canadian Archipelago with respect to RASM in Fig 5. But this assertion does not consider other systemic uncertainties present in the CryoSat-2 retrieval such as the underestimation of sea ice density for multi-year ice in recent years (Jutila et al.

2021), which might compensate the radar freeboard bias to an unknown extent. In the comparison to other SIT data sets, CryoSat-2/SMOS also yields thicker ice in the central Arctic compared to ICESat-2 estimates and though these difference are within the range of the SIT uncertainty resulting from different retrievals, an indication of SIT overestimation by CryoSat-2/SMOS remains.

LN 274: The domain averaged bias is the difference between RASM and satellite data in the region shown in Fig. 12, including all the ice regions with boundaries at DS (Davis Street), FS (Fram Strait), BSO (Barents Sea Opening) and BS (Bering Strait).

LN 277: The sentence was changed to: **The integrated sea ice growth anomalies of RASM compared to the mean 2010-2019, are displayed in Figure 7.**

LN 285-286: The sentence was changed to: **The EM ice thickness measurements on board of the Russian icebreaker „RV Kapitan Dranitzyn“ as part of the MOSAiC resupply between...**

LN 288-290: The sentence was changed to: **The main bias of the EM measurements is connected to the difficulty of instrument calibration on the ramming icebreaker. The frequent ramming operations of the ship with little progress over the undisturbed heavy ice makes processing and filtering of the ship-based measurements challenging.**

LN297-301: We replotted the satellite picture in Fig. 9 to show the leads north of Spitsbergen more clearly and added red arrows with the word ‚Lead‘.

LN 313-329: We revised the 1st part of this paragraph as follows:

Figure 10 displays the anomalies of ice convergence (top), of divergence (middle) and in the bottom panel the ice shear anomaly (all in percent/day) simulated by RASM for the JFM 2020 mean compared to the JFM 2010-2019 mean. In all three plots the transpolar drift in km/day is indicated by thick black arrows. Longer black arrows in the Davis Strait, the east coast of Greenland and the BS indicate individual grid cells with a very different drift. Blue colours in the top part of Fig. 10 indicate regions with reduced convergence and red colours in the middle part of Fig. 10 indicate those with enhanced divergence. These grid cells are likely reflecting the free-drift of thinner sea ice in marginal ice zones, where the impact of atmospheric wind forcing on the ice drift is much less limited compared to the drift within pack ice.

LN 333: OSI-SAF is explained in the text as follows: **The Ocean Sea Ice Satellite Application Facilities (OSA-SAF) deliver satellite derived scatterometer winds, sea surface temperatures and sea ice surface temperatures, radiative fluxes, sea ice concentration, edges, types and sea ice drift.**

Fig. 11 was revised. **The black arrows over the redish shading in the Eastern Arctic indicate the transpolar drift. Longer black arrows in the Davis Strait, the east coast of Greenland and the BS indicate the free-drift of grid cells within marginal ice zones.**

LN: 350: Changed to Bering Strait.

LN 363 and 369: Abbreviations were removed and physical processes are described.

LN: 401-403: Fig. 15 was replotted and enlarged. The mentioned differences at the ice edge region are now clearly visible.

We added the following sentence: **Although the greatest differences occur at the ice edge regions, remarkable changes in the central Arctic, north-west of Greenland, are visible and sea ice volume in this region is to a large extent determined by dynamical processes.**

LN: 416-419:

We added the following sentence:

Comparison of Fig. S12 with Fig. S6 indicates an inverse temperature anomaly pattern between the western and the eastern Arctic for positive and negative AO winters. Under positive AO conditions in winter (Fig. S6 exemplarily for January 2020)) negative temperature anomalies occur over the eastern Arctic and positive anomalies occur over the Canadian Basin in the western Arctic. During the negative AO winter conditions in January 2010 (Fig. S12) the eastern Arctic reveals weak positive temperature anomalies and the western Arctic negative temperature anomalies.

Answers to reviewer 2

We thank the reviewer for his/her constructive remarks. In the manuscript we identified all changes in response to the reviewer in **blue bold**.

General comments:

Point 1:

We followed the suggestion of the reviewer and described anomalies of the atmospheric MOSAiC observed parameters along the drift trajectory (10 m wind, 2m temperature, sea level pressure) compared to the climatology 2010-2019 in section 3.1.1 and **Figure S4** and meridional sea ice velocities together with the 10 m zonal and meridional wind components in **Figure S5**.

The text was changed accordingly:

***Kruppen et al. (2021)* analysed atmospheric MOSAiC in-situ measurements of 10 m winds, 2m air temperature and sea level pressure and other parameters along the MOSAiC ice drift trajectory together with ERA-5 data for the time period 2005-2020. Fig. S4 compares the 10 m wind, 2m temperature and sea level pressure along the MOSAiC drift trajectory based ERA-5 data for the climatology 2010-2019 applied in this study. Strongest deviations from the climatology occur in the time period January-March 2020. In mid-February a low surface pressure anomaly is determined by a strong synoptical cyclone event with values down to 985 hPa. This low pressure anomaly is connected with warmer temperatures and higher wind speed. Contrary high pressure values at the beginning of March 2020 are connected with cold temperatures and lower wind speed, indicating the important role of warm or cold advection for temperature changes.**

***Lei et al. (2016)* investigated the sea ice motion from the central Arctic to the Fram Strait with ice-tethered buoys between 1979-2011 and showed, that sea ice drift was determined mainly by near surface winds. They detected an accelerated meridional sea ice velocity following the Arctic Dipole (AD) pattern and a reduced meandering of the ice trajectories during the positive AD phase. The drift of the central MOSAiC Observatory was closely correlated with the ERA5 zonal and meridional components of the 10m winds (blue and red curves in Fig. S5). Compared to previous years, winds tended to have anomalies toward the Fram Strait, in particular in January, February, and March (compare red and black curves in Fig. S5, bottom), in line with corresponding sea-level pressure patterns (Fig. 2). Moreover, while the ice drift speed amounted to about 2% of the 10m wind speed on average, the drift component toward Fram Strait was positively offset compared to the winds. In particular from mid-February until the end of March, several short periods of wind toward eastern Siberia (negative values in Fig. S5, bottom) did not result in accordingly reversed drift, but only prompted the transpolar drift to pause (values close to zero in Fig. S5, bottom), likely due to the continued action of ocean currents and/or internal ice stress. From mid-June onwards, the ice drift was superimposed by pronounced inertial motions (Fig. S5), hinting at a looser ice cover (e.g., *Gimbert et al, 2012*). A close relation between the 10 m wind speed components and the sea ice velocity during the positive AO months January-March 2020 is visible. The MOSAiC drift**

showed a fast accelerated drift from the central Arctic to the Fram Strait without meandering. These results underline, that the direct fast southward MOSAiC drift towards the Fram Strait during January-March 2020 was a result of the permanent positive AO phase accompanied by a prevailing positive AD phase.

Point 2:

We agree about the importance of the Arctic Dipole for the Transpolar drift, shown by some authors and discussed this point as follows.

Besides the AO, the Arctic Dipole (AD) pattern is important for the Arctic circulation and sea-ice motion (*Wu et al., 2006; Cai et al., 2018; Watanabe et al., 2006; Zhang, 2015*). The AD pattern in its positive phase is connected with a negative pressure anomaly over the eastern Arctic and a positive pressure anomaly over the western Arctic and leads to an acceleration of the transpolar drift in agreement with *Lei et al. (2016)*. Previous studies on the AD pattern, either in summer (*Cai et al., 2018*), or in winter (*Wu et al., 2006*) often used a rather small domain (60°-90°N or 70°-90°N) and defined the AD pattern as second EOF of monthly mean SLP fields. For these small areas the domain boundaries do induce an artificial preference of particular pattern structures as discussed by *Legates (2003)* and *Overland and Wang (2010)*. Since neither EOF2 nor EOF3 of the above described analysis for the large domain 20°-90°N reveal an AD pattern, an additional EOF analysis of monthly mean SLP over the smaller domain 60°-90°N was performed, over the same 1979-2000 period as before.

Fig. S2 shows the respective first EOFs and their daily indices. The first EOF displays again the AO pattern, and the daily indices over the MOSAiC period Nov 2019 to May 2020 are highly correlated (0.95) with the AO index based on the EOF1 for the large domain (Fig. 1a) In this analysis, the AD pattern appears as third EOF, which indicates that the AD pattern is less stable than the AO pattern. The explained variances are 15 % for the second EOF and 13.6 % for the third EOF (AD). The positive AO phase from January-March 2020 is accompanied by a prevailing positive phase of the AD pattern (Fig. S2). The histogram of the daily AD indices for the period January to March 2020 indicates a higher variability of the AD index compared to the AO index (compare Fig. S1, right and S3). Whereas the AO index remain positive over the whole period January to March 2020, the AD index shows a prevailing positive phase, but with a smaller shift of the distribution towards positive values compared to the shift in the distribution of the AO index. The time series of the AD index reveals more positive values in January and March, but a shift to more neutral and negative values in February (see time series for EOF3 in S2). This behavior of the AO and AD indices explains to a large extent the differences in the monthly mean SLP pattern over the Arctic for January, February and March, displayed in Fig. 2.

We added additional citations in the references.

Special comments:

- 1) These results have been described in a recently submitted paper Krumpfen et al. (2021) and cited here.

- 2) We found it difficult and prefer to keep our wording with thermodynamic processes and combined effects of thermodynamical and dynamical changes.
- 3) LN 310: Changed to "**the SIT distribution in a region**".
- 4) LN 330: Changed to "**the climate mean of 2010-2019**".
- 5) LN 389: Changed to "**Compared to the short daily atmospheric time scales the longer time scales of ocean and sea ice processes provide memory effects for seasonal sea ice forecasts...**"
- 6) LN 430: Changed to "**losing heat to the atmosphere**"